Barrejon, M.; Primo Arnau, AM.; Gomez-Escalonilla, M.; Fierro, JLG.; García Gómez, H.; Langa, F. (2015). Covalent functionalization of N-doped graphene by N-alkylation. Chemical Communications. 51(95):16916-16919. https://doi.org/10.1039/c5cc06285c

Journal Name

COMMUNICATION

Covalent functionalization of N-doped graphene by N-alkylation†

Myriam Barrejón,[a] Ana Primo,[b] María José Gómez-Escalonilla,[a] José Luis García-Fierro,[c] Hermenegildo García*[b] and Fernando Langa*[a]

Received 00th January 20xx,
Accepted 00th January 20xx

DOI: 10.1039/x0xx00000x

www.rsc.org/

~~N-functionalization of N-doped graphene has been achieved successfully by phase transfer catalysis in combination with microwave irradiation. The derivatized N-doped graphenes were characterized using AFM, TEM, TGA and spectroscopic techniques. Importantly, the consequence of N-derivatization is a variation in the bandgap of the resulting material.~~

Nitrogen doped graphene was modified by N-alkylation using a combination of phase transfer catalysis in combination with microwave irradiation. The resulting derivatives of N-doped graphene were analysed showing that the bandgap of the material varied depending on the alkylation agent used.

Graphene (G) has emerged in the last decades as one of the most promising materials due to its unique physical and chemical properties that make it a suitable material for a broad range of applications~~.~~ ~~going~~ from microelectronics to composites.[1] Controlling the properties of G appears to be an approach of choice to expand the range of applications further, ~~Controlling G properties appears as a general methodology to expand further the range of applications~~ modulating the response of G materials. In this regard, chemical doping appears to be an obvious method for tuning the properties of G~~. appears as an obvious possibility to tune the G properties~~.[2] Two approaches have been proposed to chemically dope G: (1) functionalization on the G surface or (2) substitutional doping, which introduces heteroatoms into the carbon lattice.[1] Among various possible dopants, N-doping has become the most widely reported due to the facile doping process and the effective modulation of the electronic properties while maintaining high electrical conductivity.[3, 4] Concerning the preparation of heteroatom-doped G, chitosan, which acts as a source of carbon and nitrogen, has been used for the preparation of few layers thick N-doped G [(N)G] films and powders (containing from 0.4 to 7 wt % nitrogen) by pyrolysis ~~powders (from 0.4 to 7 wt %) by pyrolysis~~ under moderate temperatures (800-1200 ºC).[5,6] Nitrogen is a neighbour element to carbon in the periodic table. Due to its electron configuration ($1s^2 2s^2 2p^3$) does it contain 1 more electron than carbon and can as such introduce additional π-electrons into the carbon system and therefore additional n-type carriers, which could ~~in the Periodic Table and presents excessive valence electrons ($1s^2 2s^2 2p^3$), introducing additional π-electrons in the carbon system and therefore additional n-type carriers, which could~~ compensate the carrier mobility reduction caused by the defects after doping graphene.[4]

Three common bonding configurations are usually obtained when introducing nitrogen into the carbon lattice: pyridinic N, pyrrolic N and quaternary or graphitic N.[2,7] Among these configurations, the quaternary N and pyridinic N are the most common types. As mentioned above, heteroatom doping offers possibilities for tailoring the electronic properties of G. The larger electronegativity of nitrogen compared to that of carbon (3.04 *vs.* 2.55 on the Pauling scale) induces charge polarization in the carbon network conferring G with semiconducting properties. The electron-rich nature of nitrogen induces a n-type semiconducting effect and the Fermi level is shifted above the Dirac point,[8,9] thus, the band gap between the valence and the conduction band will be opened. ~~In summary, doping converts G from gapless structure to semiconductor, and this effect should increase with the doping concentration, that is, the band gap continues to grow with increasing doping concentrations.[8]~~ Therefore, N-doping provides the possibility of tuning the band gap of graphene which makes these doped materials great candidates for applications in electronic devices. [10, 11, 12] It should also be

[a] Universidad de Castilla-La Mancha, Instituto de Nanociencia, Nanotecnología y Materiales Moleculares (INAMOL), 45071-Toledo (Spain)
E-mail: Fernando.Langa@uclm.es
[b] Instituto Universitario de Tecnología Química, CSIC-UPV
Universidad Politécnica de Valencia, 46022-Valencia (Spain)
E-mail: hgarcia@qim.upv.es.
[c] Instituto de Catálisis y Petroleoquímica, CSIC
Cantoblanco, 28049-Madrid

† Electronic Supplementary Information (ESI) available: [details of any supplementary information available should be included here].See DOI: 10.1039/x0xx00000x

Please do not adjust margins

Con formato: Sangría: Izquierda: 0 cm, Sangría francesa: 0,5 cm

Con formato: Tachado

Con formato: Fuente: +Cuerpo (Calibri), Sin Negrita, Superíndice , Sin Versalitas

Con formato: Fuente: +Cuerpo (Calibri), Sin Negrita, Superíndice , Sin Versalitas

Con formato: Fuente: +Cuerpo (Calibri), Sin Negrita, Superíndice , Sin Versalitas

considered that doping could play an adverse effect by deteriorating the thermal and mechanical properties of G

Compared to doping of graphene with elements such as nitrogen, chemical functionalization of G using techniques such as alkylation are based on standard organic reactions through which a wide spectrum of functional groups can be anchored onto ~~As compared to element doping, the chemical functionalization of G with organic moieties is based on some typical organic reactions through which a wide spectrum of functional groups has been chemically anchored onto~~ G. In principle, doped G could also be modified by specific reactions at the dopant heteroatom through different routes depending on the nucleophilic or electrophilic nature of the dopant element.[2] Specifically, in the present case, pyridinic N atoms in (N)G should act as anchoring sites for N-alkylation reactions often used in organic chemistry. ~~,...~~ Since functionalization on G commonly occurs at the edges, covalent attachment through N- atoms could be a way to achieve functionalization of the basal plane of the graphene lattice. ~~Since functionalization on G use to occur at the edges, covalent attachment through N-atoms would be an effective way to get functionalization on the basal plane of the carbon lattice.~~ Phase transfer catalysis (PTC) is a versatile method to promote organic reactions between immiscible solutions due to the action of phase transfer agents facilitating interface transfer ~~due to the action of catalytic amounts of phase transfer agents, facilitating interface transfer~~ of species.[13] PTC offers several advantages, such as operational simplicity, mild reactions conditions and the environmental benignity of the reaction system. By combining microwave irradiation (MW) technology[14,15] and PTC conditions, substantial improvements can be achieved in terms of reaction efficiencies, selectivity and eco-friendly conditions.[16]

Here, we report an efficient method to synthesize N(G) sheets bearing organic addends anchored to the N pyridinic sites by combination of PTC and MW irradiation techniques. To the best of our knowledge, this is the first example of N-graphene functionalization based on derivatization of the heteroatom. In order to provide evidence of (N)G functionalization different techniques have been used, such as thermogravimetric analysis (TGA), X-Ray Photoelectron Spectroscopy (XPS), Fourier-Transform Infrared Spectroscopy (FTIR) and Raman Spectroscopy, as well as AFM measurements provided information about the sample topography. Chitosan (Aldrich, low molecular weight) previously purified from insoluble residues was pyrolyzed under Ar atmosphere at 900 ºC for 6 h. The resulting turbostratic graphitic residue ~~This turbostratic graphitic residue~~ was sonicated at 700 W for 1 h to obtain dispersed (N)G in water. The nitrogen content of the sample was 6.65 wt% as determined by elemental combustion chemical analysis. ~~The nitrogen content of the sample determined by elemental combustion chemical analysis was 6.65 wt%.~~

Covalent functionalization of (N)G suspensions with the corresponding bromide derivative was initially performed under PTC conditions by classical heating by heat diffusion (CH) (Scheme 1). N-alkylation reaction of (N)G was carried out at 70 ºC for 20 h in the presence of tetra-*n*-butylammonium bromide (TBAB) as Phase Transfer Catalyst and potassium carbonate (K_2CO_3) as base, affording functionalized graphene ***f*-NG 1-4.** The resulting materials were thoroughly washed with different solvents to remove any remaining salt and unreacted bromide derivatives.

Due to low degree of functionalization obtained under CH, the experiments were repeated employing MW irradiation. ~~As hybrids *f*-NG 1-4 showed a low degree of functionalization, according to TGA, the reactions were performed under MW heating, reducing the reaction time from 20 h to 60 min.~~ The reactions were carried out in a CEM microwave reactor in a closed quartz tube with pressure control. For the sake of comparison, the alkylation reaction on (N)G was also performed under MW irradiation, in the absence of phase transfer catalyst ~~PTC~~ (TBAB).

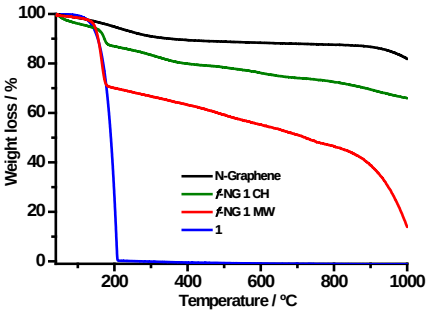

Fig. 1. . TGA curves for N-graphene (black), hybrid obtained under CH (green), hybrid obtained under MW irradiation (red) and bromide derivative (blue).

The first evidence of the successful covalent functionalization of (N)G was obtained from TGA. Fig. 1~~S2~~ shows the thermogravimetric profiles of (N)G together with those of N-alkylated graphene (N)G **1** through CH or MW heating in the presence of TBAB. For (N)G, the main weight loss takes place at around 200 ºC and it can be ascribed to the decomposition of labile oxygen-containing groups present in the material. At 600 ºC, a weight loss of around 11 % is observed which could be assigned to the removal of more stable oxygen functionalities. For *f*-**NG 1** obtained by CH, an additional weight loss of 12 % is observed at this temperature, which can be attributed to the decomposition of the addend attached to (N)G, based on the TGA profile of phenacyl bromide 1 (Fig. 1). Taking this into account, the number of groups attached to ~~the basal plane of~~ graphene was estimated 1 *per* 6.2 nitrogen or 93 carbon atoms.

Con formato: Justificado

Con formato: Fuente: +Cuerpo (Calibri), Sin Negrita, Sin Versalitas, Resaltar

Con formato: Fuente: +Cuerpo (Calibri), Sin Negrita, Sin Versalitas, Resaltar

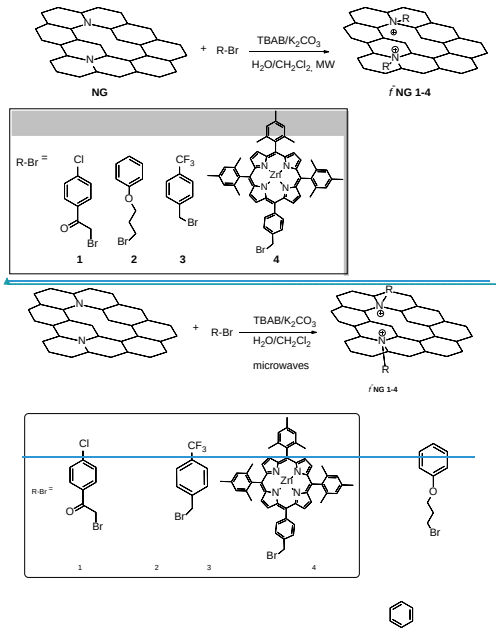

Scheme 1. Synthetic route towards *f*-**NG 1-4**.

In the case of the thermogram obtained for the N-alkylation under MW irradiation, the additional weight loss observed for *f*-**NG 1** at 600 ºC is approximately 33 %, which corresponds to the presence of 1 group *per* 2.2 nitrogen atoms or 34 carbon atoms. The thermogravimetric profile of the control sample of *f*-**NG 1** obtained by MW heating in the absence of PTC shows a weight loss of 23 %, indicating that the degree of functionalization is proportionally lower (see ESI, Fig. S1). Weight losses corresponding to the rest of (N)G hybrids **2-4** bearing different groups (Scheme 1) are found in Fig. S2 and Table S1. As observed, reactions performed under MW heating not only reduced significantly the reaction times but also gave rise to materials with higher degrees of functionalization in respect to classical heating. It is interesting to note that the highest percentage of functionalization correspond to about 44 % of the total N atoms present on (N)G determined by combustion elemental analysis.

Further support on the covalent anchoring of the functional groups on the (N)G surface was provided by XPS measurements (see Tables S2, S3 and Fig. S3). Two types of normal emission angle-integrated scans were carried out for the samples in this study: low resolution survey scans from 200 to 1300 eV and pass energy in the analyzer of 100 eV, and high resolution scans 15-20 eV windows and 50 eV pass energy. The survey scans were primarily used to monitor samples for the presence of surface contaminants. High resolution scans were acquired for the C 1s, O 1s, N 1s and Zn 2p energy regions.

Table S3 lists the elements detected and their percentage determined by XPS. The elements detected by XPS are in agreement with the nature of the organic addend. One interesting point to note is that the atomic percentage of N determined by XPS is much lower than the value determined by chemical analysis. It should be noted, however, that elemental quantification by XPS is problematic since it only provides analysis of the surface layers (up to *ca.* 3 nm) of powders and it could be that N atoms are not homogeneously distributed between the surface and bulk when (N)G is analyzed as dry powders. In addition, functionalization can mask some N atoms that will be covered by the substituent. As expected, the N content of *f*-**NG 4** increases due to porphyrin nitrogen atoms. Evidence of the covalent attachment of the organic addends to *f*-**NGs** is provided by the FTIR spectra (Figs. 2~~1~~ and S4). Accordingly, *f*-**NG 1** shows features that do not appear in the starting (N)G, such as two bands at 1691 cm^{-1} and 1400 cm^{-1} attributable to the C=O and C-N stretching vibration modes, respectively. In addition, a new band appeared at 699 cm^{-1} which was attributed ~~a new band appears at 699 cm^{-1} which is attributed~~ to the C-Cl stretching. The effective attachment~~grafting~~ of the bromide derivative is further confirmed by the increase of the aliphatic C-H stretching bands at 2910-2960 cm^{-1}. FTIR spectra for the rest of hybrids showed similar results after functionalization (see ESI, Fig. S4).

Raman measurements show the characteristic D and G bands at around 1350 cm^{-1} and 1594 cm^{-1} respectively (see Fig. S5 in ESI). The D band shows a high intensity, indicating a high density of defects within the hybrid structure.[6] This is in concordance with the small graphene crystallite size of around 20 nm.[17] A higher N content implies a higher number of defects (higher I_D/I_G) combined with smaller crystallites. In addition, a general distortion of the 2D band was observed for all the hybrids. In this regard, previous studies have shown that the Raman bands get broadened and the 2D band disappeared when increasing the doping concentration.[18] No differences were observed between the Raman spectra of the starting (N)G and those corresponding to the functionalized hybrids, indicating that N-functionalization did not influence on the density of defects on the G sheet.

The ^{1}H-NMR spectrum of *f*-**NG 1** recorded in $CDCl_3$ is presented in Fig. 2. ~~As it can be seen there,~~ it was possible to record the signals corresponding to the 4-chlorophenacyl units in the aromatic region as well as the singlet of the methylene group appearing at 5.30 ppm. This chemical shift was~~is~~ different from that of the 4-chlorophenacyl bromide used as reagent (4.42 ppm) and would be about 1.3 ppm upfield with respect to the value reported for N-(4-chlorophenacyl)pyridinium, a structurally close analog of the subunits present in *f*-**NG 1**, that is 6.66 ppm. This strong upfield shift would be compatible with the influence that the anisotropy of the π-cloud of graphene exerted~~s~~ on this CH_2 group.

Código de campo cambiado

Con formato: Fuente: +Cuerpo (Calibri), Sin Negrita, Superíndice , Sin Versalitas

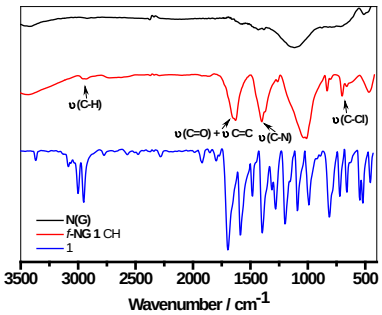

Fig. 2 FT-IR spectra of **(N)G** and *f*-**NG 1** compared with its bromide precursor 1.

The UV-vis absorption spectra for N(G) show the dominant absorbance peak around 200 nm, which was~~is~~ ascribed to π-π* transition of aromatic C–C bonds, and a shoulder at 280 nm, associated with n-π* transition of C=O bonds[19] (see ESI, Fig. S7). For *f*-**NG 1**, a new peak ~~is observed~~was observed at around 230 nm which could be attributed to the anchored addend, since its absorption spectrum shows a sharp peak at this wavelength. For *f*-**NG 2** and *f*-**NG 3** no supporting ~~helpful~~ information could~~can~~ be obtained from the UV-vis spectra, since the peaks corresponding to the addends overlap~~fall just~~ with the dominant absorbance peak from (N)G.

However, for *f*-**NG 4** (see ESI, Fig. S8), the UV-vis spectrum shows a new absorption peak at 428 nm, which was~~is~~ attributable to the π-π* transition of the porphyrin unit. As observed, this peak was~~is~~ bathochromically shifted by 4 nm with respect to 4. This suggested~~s~~ the existence of electronic interactions between porphyrins and the basal plane of (N)G.

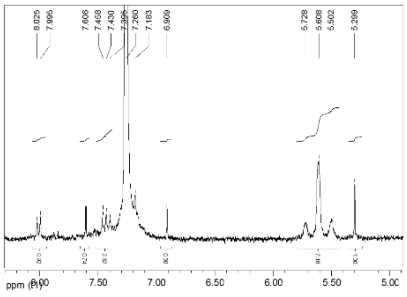

Fig. 2 Expansion of the ^{1}H-NMR spectrum recorded for *f*-**NG 1** in $CDCl_3$ (see Fig. S6 in the ESI for the full spectrum).

In order to probe the excited-state interactions between the porphyrin and graphene, fluorescence spectra of the hybrid *f*-**NG 4** and precursor 4 were compared (see ESI, Fig. S8b). Both solutions were prepared in THF optically matched at the selected excitation wavelength and their emission spectra were acquired. Upon excitation of 4 at the Soret band (426 nm), a fluorescence emission was~~is~~ observed at 494 nm. A weaker fluorescence emission was~~is~~ observed when the hybrid *f*-**NG 4** was~~is~~ excited at the same wavelength. The calculated quenching efficiency was~~is~~ around 40 %, suggesting the existence of photoinduced electron transfer from the porphyrin 4 to (N)G. AFM images, as illustrated in Fig. 3, reveal the presence of few layer graphene flakes with an average height of ca. 1.5 nm, which correspond to an approximately four layers thick structure ~~which correspond to approximately four layer thick structures~~.[20] It could also be that the thickness of N-doped graphene could be somewhat larger than that of pristine graphene sheets. Anyway, this thickness clearly evidenced~~s~~ the strongly exfoliated character of the sample. Further, the isolated layers showed polygonal shapes which are very characteristic in graphene samples. Finally, it is worthy to mention that comparing the images from the starting (N)G (top panel) and *f*-**NG 4** (bottom panel), the last shows brightened zones whose height coincides with the distance calculated for the porphyrin unit, which could suggest the presence of the porphyrin attached to ~~the basal plane of~~ graphene, although additional evidence by Zn mapping on high resolution TEM image of *f*-**NG 4**, would provide additional evidence to this proposal.

Con formato: Fuente: Sin Negrita

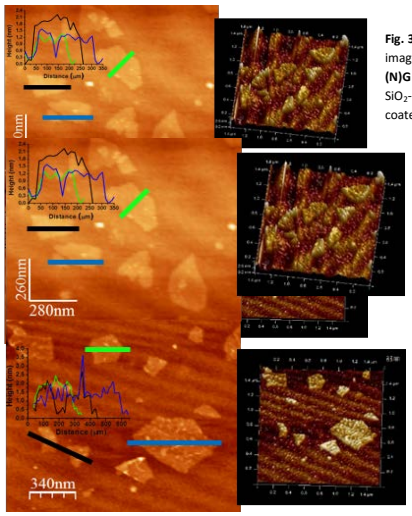

Fig. 3 AFM image of **(N)G** on SiO_2-coated Si wafers and 3D image on the right side (top panel). AFM image of *f*-**NG 4** and 3D image on the right side (bottom panel).

Transmission electron microscopy (TEM) was performed in order to obtain detailed views of their morphology and analyze their possible crystal structure. TEM images obtained for (N)G and *f*-**NG 4** are shown in Fig. S9. (N)G exhibits wrinkled paper-like morphology (Fig. S9a). Magnified images reveal the

presence of few-layers thick graphene with a detailed crystalline structure (Fig. S9b). The selected area electron diffraction (SAED) pattern given in Fig. S9c further supports the high crystallinity of (N)G, showing a symmetric hexagonal diffraction pattern, which is ascribed to a typical diffraction pattern of graphite.[21,22] As observed for *f*-**NG_–4**, chemical modification induces morphological changes on the surface (Figs. S9d and S9e), and the crystalline structure is disrupted after functionalization with the porphyrin unit (4) (Fig. S9e). This decrease of the crystallinity is further confirmed by the SAED pattern (Fig. S9f) that shows ring-like diffraction spots, probably due to structure distortion caused by intercalation of porphyrin into its graphitic planes.[23]

Assuming the materials to be semiconductors, a plot of the Kubelka-Munk function *vs.* hν affords the band gap energies. The optical band gaps of the new hybrids were determined using the Tauc plot[24] of the modified Kubelka-Munk function with a linear extrapolation (Fig. 4). The approximated band gap of (N)G was found to be 4.12 eV and 3.35 eV, 3.50 eV, 3.20 eV and 3.79 eV for *f*-**NG 1-4**, respectively. The variation of the band gap after N-functionalization in these materials could be attributed to the disruption of graphene sublattices and the changes in the electronic density at the N atoms. Since band gap engineering is one of the high priority goals in the development of graphene electronics, the experimental influence of optical band gap as a function of the substituent on N atom appears as a new general method to tune the optical band gap by functionalization ~~on the basal plane~~of graphene.

In summary, ~~we have performed successfully the~~ unprecedented N-functionalization of N-doped graphene with a variety of organic addends by ~~a~~ phase transfer catalysis in combination with microwave irradiation is reported~~is essential for an efficient functionalization. The N-graphene derivatives were characterized by AFM, TEM, TGA and spectroscopic techniques~~. As result of this covalent functionalization, variations in the bandgap of the functionalized doped graphene were observed. The methodology here described should be also applicable for other dopant elements and should constitute a new general strategy for ~~basal~~ functionalization of graphene~~. Further work is currently being undertaken in this direction~~.

Financial support from Mineco (Spain) (CTQ2013-48252-P and CTQ2012-32315), Junta de Comunidades de Castilla-La Mancha (PEII-2014-014-P) and Generalidad Valenciana (Prometeo 13/19) is gratefully acknowledged. One of us (MB) thanks to a FPI grant from Mineco.

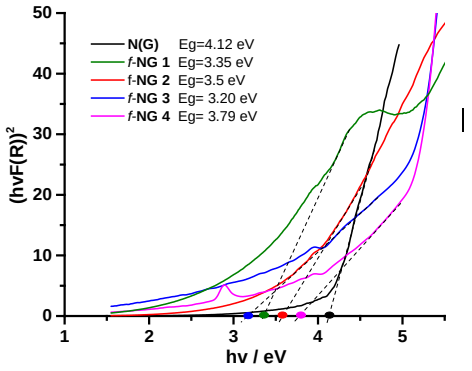

Fig. 4 Tauc plot to determine the optical band gap of **(N)G** compared to that of *f*-**NG 1-4**

Notes and references

1 H. Wang, T. Maiyalagan and X. Wang, *ACS Catal.*, 2012, **2**, 781.
2 a) S. Navalón, A. Dhakshinamoorthy, M. Álvaro and H. García, *Chem. Rev.,* 2014, **114**, 6179. b) L. Rodríguez-Pérez, M. Á. Herranz, N. Martín, *Chem. Commun*, 2013, **49**, 3721.
3 D. Wai, Y. Liu, Y. Wang, H. Zhang, L. Huang and G. Yu, *Nano Lett.,* 2009, **9**, 1752.
4 W. J. Lee, U. N. Maiti, J. M. Lee, J. Lim, T. H. Han and S. O. Kim, *Chem. Commun.*, 2014, **50**, 6818.
5 A. Primo, P. Atienzar, E. Sánchez, J. M. Delgado, H. García, *Chem. Commun,* 2012, **48**, 9254.
6 A. Primo, E. Sánchez, J. M. Delgado and H. García, *Carbon*, 2014, **68**, 777.
7 X. Wang, G. Sun, P. Routh, D-H Kim, W. Huang and P. Chen, *Chem. Soc. Rev.*, 2014, **43**, 7067.
8 M. Wu, C. Cao and J. Jiang, *Nanotechnology*, 2010, **21**, 505202.
9 P. Rani and V.K. Jindal, *RSC Adv.*, 2013, **3**, 802.
10 M. Latorre-Sanchez, A. Primo, P. Atienzar, A. Forneli and H. García, *Small*, 2015, **11**, 970.
11 M. Gupta, N. Gaur, P. Kumar, S. Singh, N.K. Jaiswal and P.N. Kondekar, *Phys. Lett. A*, 2015, **379**, 710.
12 H.S. Kim, H.S. Kim, S.S. Kim and Y.H. Kim, *Nanoscale*, 2014, **6**, 14911.
13 S. Shirakawa, K. Maruoka, *Angew. Chem. Int. Ed.*, 2013, **52**, 4312.
14 a) P. de la Cruz, F. Langa, *Comb. Chem. High T. Scr.*, 2007, **10**, 766. b) F. Langa, P. de la Cruz, E. Espíldora, J.J. García, M.C. Pérez-Rodríguez and A. de la Hoz, Carbon, 2000, **38**, 1641-1646.
15 K. C. Oliver Kappe, *Angew. Chem. Int. Ed.*, 2004, **43**, 6250.
16 G. Keglevich, A. Grün and E. Bálint, *Current Organic Synthesis*, 2013, **10**, 751.
17 Z. H. Ni, L. A. Ponomarenko, R. R. Nair, R. Yang, S. Anissimova, I. V. Grigorieva, F. Schedin, P. Blake, Z. X. Shen, E. H. Hill, K. S. Novoselov and A. K. Geim, *Nano Lett.*, 2010, **10**, 3868.
18 C. Chang, S. Kataria, C. Kuo, A. Ganguly, B. Wang, J. Hwang, K. Huang , W. Yang, S. Wang, C. Chuang, C. Huang, W. Pong, K. Song, S. Chang, J. Guo, Y. Tai, M. Tsujimoto, S. Isoda, C. Chen, L. Chen and K-H Chen, *ACS Nano*, 2013, **7**, 1333.
19 T. V. Cuong, V. H. Pham, Q. T. Tran, S. H. Hahn, J. S. Chung, E. W. Shin and E. J. Kim, *Mater. Lett.*, 2010, **64**, 399.

Con formato: Fuente: +Cuerpo (Calibri), Sin Negrita, Español (España), Sin Versalitas, Escala de caracteres 105%
Con formato: Fuente: +Cuerpo (Calibri), Sin Negrita, Español (España), Sin Versalitas, Escala de caracteres 105%
Con formato: Fuente: Sin Negrita, Español (España), Sin Versalitas
Código de campo cambiado
Con formato: Español (España)
Con formato: Sin subrayado, Color de fuente: Automático, Español (España)
Con formato: Español (España)
Con formato: Español (España)
Con formato: Español (España)
Con formato: Fuente de párrafo predeter., Inglés (Reino Unido)
Con formato: Fuente de párrafo predeter., Español (España)
Con formato: Sin subrayado, Color de fuente: Automático, Español (España)
Con formato: Fuente: Cursiva, Sin subrayado, Color de fuente: Automático, Español (España)
Código de campo cambiado
Con formato: Fuente: Cursiva, Sin subrayado, Color de fuente: Automático, Español (España)
Con formato: Sin subrayado, Color de fuente: Automático, Español (España)
Con formato: Fuente: Negrita, Sin subrayado, Color de fuente: Automático, Español (España)
Con formato: Sin subrayado, Color de fuente: Automático, Español (España)
Con formato: Español (España)

20 Y. K. Koh, M-H Bae, D. G. Cahill and E. Pop, *ACS Nano*, 2011, **5**, 269.
21 A. Reina, X. Jia, J. Ho, D. Nezich, H. Son,V. Bulovic and M. S. Dresselhaus, J. Kong, *Nano Lett*., 2009, **9**, 30.
22 C.T. Pan, J. A. Hinks, Q. M. Ramasse, G. Greaves, U. Bangert, S. E. Donnelly, S. J. Haigh, Scientific Reports, 2014, **4**, 6334.
23 Y-F. Lu, S-T. Lo, J-C. Lin, W. Zhang, J-Y. Lu, F-H. Liu, C-M. Tseng, Y-H. Lee, C-T. Liang and L-J. Li, *ACS Nano* 2013, **7**, 6522.
24. J. Tauc, R. Grigorovici and A. Vancu*, Phys. Status Solidi*, 1966, **15**, 627.